Materials Today Bio 19 (2023) 100593

Contents lists available at ScienceDirect

Materials Today Bio

journal homepage: www.journals.elsevier.com/materials-today-bio

Soft topographical patterns trigger a stiffness-dependent cellular response to contact guidance

Jordi Comelles [a,c,**], Vanesa Fernández-Majada [a,d], Verónica Acevedo [a], Beatriz Rebollo-Calderon [a], Elena Martínez [a,b,c,*]

[a] Biomimetic Systems for Cell Engineering Laboratory, Institute for Bioengineering of Catalonia (IBEC), The Barcelona Institute of Science and Technology (BIST), Baldiri Reixac 15-21, 08028, Barcelona, Spain
[b] Centro de Investigación Biomédica en Red (CIBER), Av. Monforte de Lemos 3-5, Pabellón 11, Planta 0, 28029, Madrid, Spain
[c] Department of Electronics and Biomedical Engineering, University of Barcelona (UB), Martí I Franquès 1, 08028, Barcelona, Spain
[d] Department of Pathology and Experimental Therapeutics, University of Barcelona (UB), Feixa Llarga, 08907, L'Hospitalet de Llobregat, Spain

ARTICLE INFO

Keywords:
Contact guidance
Stiffness
Topography
Cell migration

ABSTRACT

Topographical patterns are a powerful tool to study directional migration. Grooved substrates have been extensively used as *in vitro* models of aligned extracellular matrix fibers because they induce cell elongation, alignment, and migration through a phenomenon known as contact guidance. This process, which involves the orientation of focal adhesions, F-actin, and microtubule cytoskeleton along the direction of the grooves, has been primarily studied on hard materials of non-physiological stiffness. But how it unfolds when the stiffness of the grooves varies within the physiological range is less known. Here we show that substrate stiffness modulates the cellular response to topographical contact guidance. We find that for fibroblasts, while focal adhesions and actin respond to topography independently of the stiffness, microtubules show a stiffness-dependent response that regulates contact guidance. On the other hand, both clusters and single breast carcinoma epithelial cells display stiffness-dependent contact guidance, leading to more directional and efficient migration when increasing substrate stiffness. These results suggest that both matrix stiffening and alignment of extracellular matrix fibers cooperate during directional cell migration, and that the outcome differs between cell types depending on how they organize their cytoskeletons.

1. Introduction

The ability of a cell or group of cells to migrate directionally as a response to external cues is crucial in multiple physiological and pathological processes [1–3]. For example, directional cell migration is needed for neural crest and primordial germ cell migration in development, for immune response, for wound healing, or for cell invasion in cancer metastasis among other processes. Mostly, directed cell migration has been attributed to chemotaxis, the well-studied ability of cells to follow chemical factors dissolved in the environment. However, directed cell migration can also be driven by mechanical cues (*durotaxis*) [4] or even topographical features. This last form of directed cell migration is known as contact guidance [5,6]. Contact guidance results from the presence of micron and sub-micron aligned structures formed by the cellular rearrangement of extracellular matrix (ECM) protein fibers (typically collagen and fibronectin). Such protein rearrangement can be found *in vivo* in the basal membrane of healthy tissues where it is known to assist tissue formation [7,8]. On the other hand, fiber alignment can also be found in the stromal tissue around solid tumors [9], where it is identified as a negative prognostic factor [10]. In this situation, aligned fibers in the extracellular matrix regulate cell extrusion and invasion [11]. Even if the outcome of contact guidance on cell migration is well known, how the geometrical features are sensed by cells and transduced in directional migration is not fully comprehended.

In vitro, contact guidance has been studied by culturing cells on grooved substrates. There, cells elongate, align, and migrate in the

* Corresponding author. Biomimetic Systems for Cell Engineering Laboratory, Institute for Bioengineering of Catalonia (IBEC), The Barcelona Institute of Science and Technology (BIST), Baldiri Reixac 15-21, 08028, Barcelona, Spain.
** Corresponding author. Biomimetic Systems for Cell Engineering Laboratory, Institute for Bioengineering of Catalonia (IBEC), The Barcelona Institute of Science and Technology (BIST), Baldiri Reixac 15-21, 08028, Barcelona, Spain.
E-mail addresses: jcomelles@ibecbarcelona.eu (J. Comelles), emartinez@ibecbarcelona.eu (E. Martínez).

https://doi.org/10.1016/j.mtbio.2023.100593
Received 14 October 2022; Received in revised form 20 February 2023; Accepted 22 February 2023
Available online 27 February 2023

direction of the grooves mimicking the *in vivo* phenotype on top of ECM fibers. Topographically induced contact guidance has been extensively reported for several cell types: fibroblasts [12–18], epithelial [12,18–20], endothelial [21,22], neuronal [12,23,24], and muscle cells [25,26]; as well as stem cells [27,28] and cancer cells [29–34]. Early on, microtubule and actin cytoskeletons were observed to align with the topographical grooves [13–15,19,27,34–36]. Later on, it was reported that grooves lead to the alignment of focal adhesions and the activation of Focal Adhesion Kinase (FAK) and downstream signaling to reorganize actin cytoskeleton [19–21,31,33,37]. Such reorganization should lead to higher traction forces in the direction of the grooves. Therefore, the cell contractility machinery seems to be playing a part, involving the Ras homolog family member A (RhoA) pathway [21,26,28,31]. However, most of the reported work so far has been performed on topographically modified stiff materials such as thermoplastic polymers and polydimethylsiloxane (PDMS) [19–22,25,26,28,31,33]. These materials have elastic modulus values of $\sim 10^6$ kPa, which are much harder than the ones encountered in soft tissues *in vivo*, either in physiological or pathological conditions [38,39], which range from 0,1–100 kPa. Bearing in mind that substrate stiffness regulates cell size and shape [40,41], focal adhesion formation [42], and actin and microtubule cytoskeletons' organization [40,41,43,44] – that are main hallmarks of contact guidance –, as well as the ability of cells to exert tractions on the underlaying substrate [45]; it appears that the elasticity of the substrate can be important for regulating contact guidance, but it has been mainly overlooked. Within this scenario, there is the need to study contact guidance while acknowledging substrate stiffness. In particular within the context of cancer disease, where changes on both ECM architecture and stiffness are reported [46,47], studying the effects of both cues on the migratory behavior of the stromal and cancer cells (both invasive and non-invasive) can be key in understanding the disease progression.

Up to date, contact guidance studies on soft materials have been hampered by the lack of proper microfabrication methods to create well-controlled micron and sub-micron features on such materials. In fact, only a few examples can be found in literature where topographical grooves are introduced on soft substrates [34,48–50]. These studies have shed some light on their effects on cancer cells, fibroblasts and T-cells in soft environments. Fibroblasts showed elongation and directional migration on aligned soft matrices [48], cancer cells responded differently to soft (2.3 kPa) than to stiff (50 kPa) topographical grooves [34], and T-cells experienced contact guidance on soft (16 kPa) but not on stiff (50 kPa) substrates [49]. However, whether a reduction of stiffness would abrogate directional migration through the decrease of cell traction, or an increase of stiffness would enhance directional response of epithelial cells are relevant questions yet to be solved. Thus, the systematic study of contact guidance within the *in vivo* stiffness range is crucial to explore new strategies to tackle scenarios where topographically induced directed migration takes place *in vivo*, such as cancer disease. Here, we use a mesenchymal cell line and two epithelial cancer cell lines (invasive and non-invasive) to study the response of contact guidance associated hallmarks, cell elongation, alignment and directional migration, to systematic changes of the substrate stiffness covering physiological, pathological and non-physiological values (Fig. 1a). To that end, micron-size grooves onto polyacrylamide (PAA) hydrogel substrates were produced by using a recently developed microfabrication method [51]. Our results show that migratory mesenchymal-like cells exhibit stiffness-independent directional migration by contact guidance. This is achieved by modifying the cytoskeleton elements involved in a stiffness dependent manner. On the contrary, breast carcinoma epithelial cells exhibit stiffness-dependent directional migration by contact guidance, with an increased efficiency upon matrix stiffening. Importantly, this stiffness-dependent enhanced migration is observed in both invasive and non-invasive breast cancer cells. Strikingly, not only single cells but also cell clusters are shown to perform directional collective migration upon matrix stiffening. Altogether, these findings highlight the importance of substrate stiffness in contact-guidance associated migration and open new avenues to investigate cancer cell invasion accounting for the cooperation between matrix stiffening and ECM fiber alignment.

2. Materials and methods

2.1. Experimental design

To explore the impact of substrate stiffness on the ability of topography to influence cellular alignment and contact guided migration, we cultured mesenchymal and epithelial cells on 2 μm wide and 1 μm deep topographical grooves and ridges made of PAA gels of different stiffness (3–145 kPa). Detailed steps are described below.

2.2. Cell culture

NIH 3T3 mouse embryonic fibroblasts, MDA-MB-231 and T47D cells were obtained from ATTC. NIH 3T3 fibroblasts and MDA-MB-231 epithelial cells were grown with DMEM (Invitrogen) medium supplemented with 10% Fetal Bovine Serum (FBS) (Life Technologies), 1% L-glutamine (Gibco), 1% penicillin-streptomycin (Sigma-Aldrich), 1% sodium pyruvate (Invitrogen) at 37 °C, and 5% CO_2. Cells were passaged every 2–3 days. T47D cells were grown with RPMI-1640 medium (Invitrogen) supplemented with 10% FBS at 37 °C, and 5% CO_2. Cells were passaged every 2–3 days. For the experiments employing NIH 3T3 and MDA-MB-231, 50,000 cells per well (35 mm petri dish) were cultured on the PAA gels during 24 h. For the experiments employing T47D, 75,000 cells per well (35 mm petri dish) were cultured on the PAA gels during 24 h.

2.3. Polyacrylamide gel fabrication and microstructuring

PAA microstructured gels were prepared following the experimental procedure described in Ref. [51]. Briefly, we first prepared PDMS (Sylgard 184 Silicon Elastomer, Dow Corning) molds (5 mm in diameter containing 2 μm width and 1 μm high grooves, these dimensions were selected to be as close as possible to *in vivo* ECM fibers [33] while assuring a faithful replica of the features [51]) and spacers (10 mm in diameter). Then, 35 mm bottom glass petri dishes (MatTek) were silanized with 3-(aminopropyl)trimethoxysilane (Sigma-Aldrich) following the procedure described in Ref. [52]. Afterwards, the PDMS spacer was placed on the silanized glass of the petri dish, filled with 50 μL of polyacrylamide solution (see Supplementary Table S19) and covered with a poly (ethylene naphtalate) (PEN) (Goodfellow) sheet with the PDMS mold attached. PAA gels were then kept at room temperature (RT) with a small weight on top of the PEN sheet for 2 h to polymerize. The polymerized gels were demolded by carefully removing the flexible mold and then stored in PBS at 4 °C until further use, allowing them to achieve equilibrium swelling. Once equilibrium was reached, the stiffness of the substrates was assessed by AFM as described in Ref. [51].

Before cell seeding, fibronectin from bovine serum (Sigma-Aldrich) was covalently bound to PAA gels using Sulfo-SANPAH reagent (Sigma-Aldrich). PBS was removed and then, we freshly prepared a Sulfo-SANPAH solution at a concentration of 2 μg μL^{-1} in Milli-Q water and added 50 μL on top of each hydrogel. The PAA gels with the Sulfo-SANPAH solution were UV-irradiated (Light Source LQ-HXP 120 UV, LEJ) for 60 s and then rinsed several times with PBS. Next, we incubated the proteins on the activated gels using 50 μL of a 20 μg mL^{-1} fibronectin solution for 1 h at RT. Functionalized gels were stored in culture medium until cell seeding. Rhodamine-fibronectin (Cytoskeleton Inc.) was used to visualize the protein coating.

2.4. Immunostaining

Cells were fixed with 10% neutralized formalin (Sigma -Aldrich) for 35 min at 4 °C and washed three times with PBS. Cells were then permeabilized with 0.5% Triton X-100 (Sigma) for 30 min and blocked for at

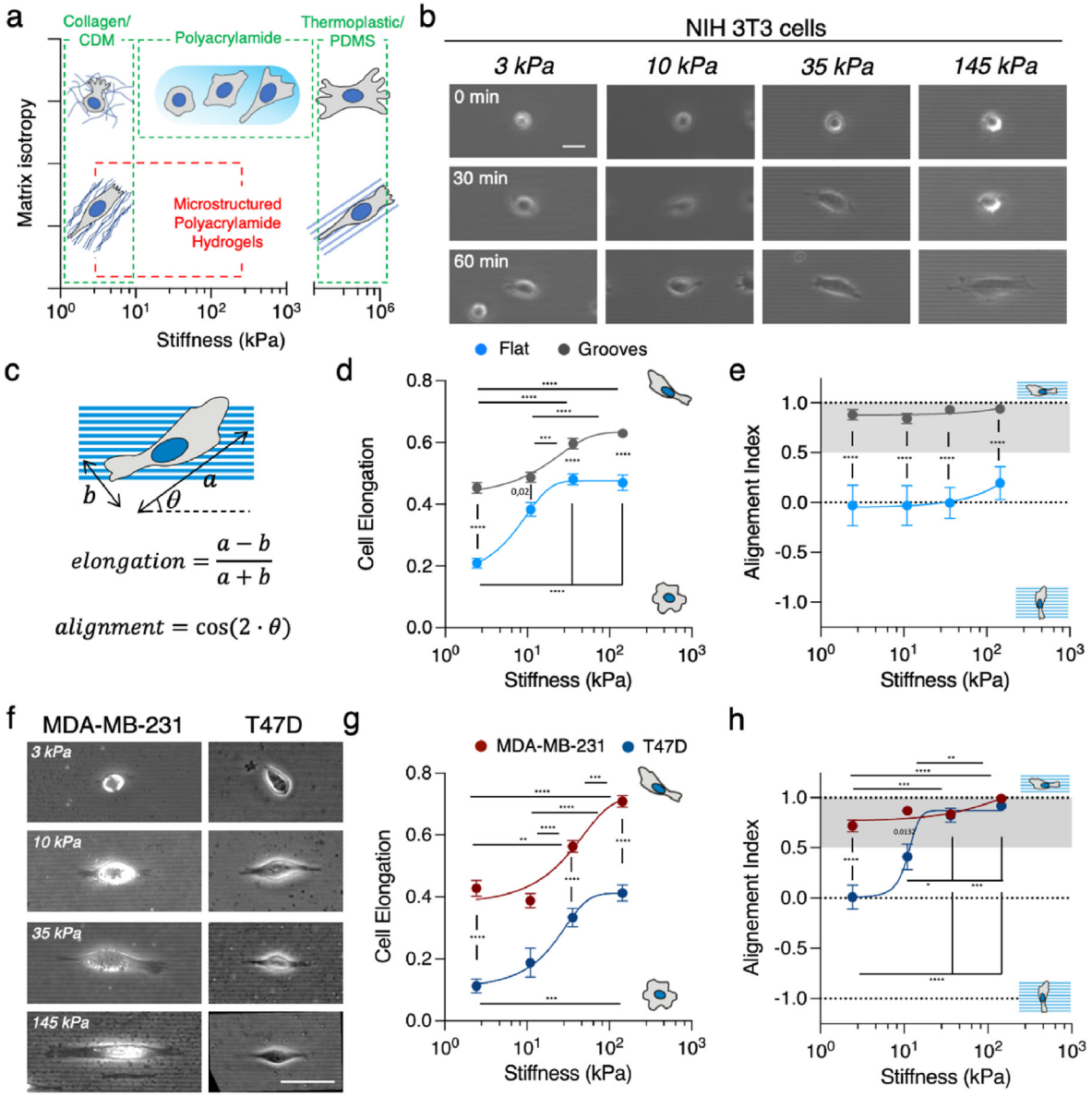

Fig. 1. Substrate stiffness modulates topographical contact guidance. (**A**) Schematics of matrix isotropy across a wide range of substrate stiffness (CDM: Cell derived matrix). (**B**) Snapshots of NIH 3T3 fibroblasts adhering, elongating and aligning on grooves of different stiffness. Scale bar, 20 μm. (**C**) Scheme depicting cell long axis a, short axis b and the angle between the long axis and the grooves θ. (**D**) Cell elongation and (**E**) cell alignment index as a function of the substrate stiffness. (**F**) MDA-MB-231 and T47D single cells spread on polyacrylamide gels with topographical grooves and ridges of increasing stiffness. Scale bar, 50 μm. (**G**) Cell elongation and (**H**) Alignment index as a function of substrate stiffness. Shadowed regions in (E) and (H) correspond to angles <30°. Data points (Mean ± SE) were fitted as an eye-guide. Statistical significance was assessed by Tukey's tests (**D**, **G** and **H**) and Kruskall-Wallis' test (**E**). NIH 3T3 cells N ≥ 3 experiments per condition and n ≥ 50 cells per condition. MDA-MB-231 N ≥ 2 experiments per condition and n ≥ 58 cells per condition. T47D cells N ≥ 2 experiments per condition and n ≥ 22 cells per condition. See Tables S1–S3 for the exact number of cells and experiments.

least 2 h with a blocking buffer containing 1% BSA (Sigma), 3% donkey serum (Millipore), and 0.2% Triton X-100 in PBS. All samples were incubated with the primary antibodies overnight at 4 °C, followed by a 2 h incubation at RT with secondary antibodies, and phalloidin rhodamine (Cytoskeleton) to stain filamentous actin (F-actin) (1:140). Finally, 30 min incubation with 4′,6-diamidino-2-phenylindole (DAPI, Life Technologies) (1:1000) for nuclei staining was employed. After three PBS washes, samples were kept in Fluoromount-G mounting media (SouthernBiotech) and stored in a humid chamber at 4 °C until imaged.

2.5. Antibodies

As primary antibodies we used purified mouse *anti*-Paxillin (Bd Biosciences) to stain for Paxillin at focal adhesions (1:100), recombinant Alexa Fluor 488 anti-alpha Tubulin antibody (Abcam) to stain microtubules (1:250) and rabbit polyclonal to Myosin light chain (phospho S20) antibody (Abcam) to stain phosphorilated-myosin (1:200). The secondary antibody employed was Alexa Fluor 647 donkey anti-mouse (Invitrogen) (1:500).

2.6. Live-cell fluorescence labelling

Imaging of actin cytoskeleton and microtubule network in live cell experiments was performed using NIH 3T3 stable cell line expressing Lifeact-GFP (Addgene) treated with SiR-tubulin (Spirochrome). NIH 3T3 fibroblasts were transfected with Lifeact-GFP using Lipofectamine 2000 (Life Technologies) and selected using geneticin G418 antibiotic (ThermoFischer). Fibroblasts expressing Lifeact-GFP were seeded on the PAA

gels and cultured for at least 12 h. Then, cell culture media was replaced by fresh media containing 100 nM SiR-tubulin and incubated for 12 h. After that, cells were imaged under the microscope at 37 °C in a humidified atmosphere containing 5% CO_2.

2.7. Image acquisition

Phase contrast images were acquired using a Nikon Eclipse Ts2 with x10 (ADL Ph1 0.25 NA) and x20 (ADL Ph1 0.40 NA) objectives. Migration experiments were performed by using phase contrast microscopy using an Axio Observer 7 (Carl Zeiss) using a x10 objective acquiring an image every 5 min for 6 h at 37 °C and 5% CO_2. Live-cell imaging of actin and microtubules was performed using an Axio Observer 7 (Carl Zeiss) using a x63 objective. Immunostained samples were observed using confocal laser scanning microscope (LSM 800, Zeiss) equipped with a x63 oil objective (NA 1.40) and a x100 oil objective (NA 1.40).

2.8. Cell morphology evaluation

The effects of both stiffness and topography were established by measuring morphological parameters using Image J software (http://rsb.info.nih.gov/ij, NIH). Cell area was measured by outlining the cell shape. Cell elongation and alignment were measured by fitting an ellipse to the cell shape. The elongation was assessed by calculating $(a-b)/(a+b)$, being a and b the ellipse major and minor axis, respectively. The alignment index was calculated as $cos\,(2\bullet\theta)$ where θ is the angle between the ellipse's major axis and the direction of the topographical pattern (Fig. 1c) or the laboratory framework in the case of flat surfaces. T47D cell clusters area was evaluated by outlining the cluster's shape and measuring its area.

2.9. Cell migration evaluation

The centroid trajectories of NIH 3T3 cells, MDA-MB-231 cells and T47D single cells were tracked using the Manual Tracking Plug-in in Fiji (http://rsb.info.nih.gov/ij, NIH, USA). For T47D clusters, each cluster was outlined, and its centroid was calculated with Fiji. Data analysis was performed using a custom-made code in Matlab (Mathworks, USA). Cell centroid positions during the experiment were defined as $(x(t_i), y(t_i))$, being $t_i = i \bullet \Delta t$ with $i = 0, \ldots, n$ and Δt the time between consecutive images. The total distance covered by the cells was computed as $\sum_{i=1}^{n}\sqrt{(x(t_i)-x(t_{i-1}))^2+(y(t_i)-y(t_{i-1}))^2}$ and the net distance as the vector difference between the initial and the final point $\vec{d} = (x(t_n) - x(t_0), \quad y(t_n) - \quad y(t_0))$, being its module $d = \sqrt{(x(t_n)-x(t_0))^2+(y(t_n)-y(t_0))^2}$. The alignment of each trajectory was computed by averaging the alignment of the vector displacement between two consecutive time-points and the topographical pattern for every time-point $\langle \cos\,(2\bullet\alpha(t_i))\rangle_i$, being $\alpha(t_i)$ the angle between the vector defined by two consecutive cell positions $(x(t_i)-x(t_{i-1}), y(t_i)-y(t_{i-1}))$ and the direction of the grooves. This index equals 1 when the trajectory is parallel to the direction of the grooves, 0 when is random and −1 when it is perpendicular.

2.10. Focal adhesion analysis

To characterize focal adhesion size, shape and orientation, fluorescent images of paxillin were treated using Fiji as follows. First, a median filter was applied and the background signal subtracted. Then, a contrast-limited adaptive histogram equalization (CLAHE) was used, and the background was again removed using an exponential function. Finally, a Laplacian of Gaussian filter was applied to the resulting image and the focal adhesions were selected with auto-threshold function. Orientation of the focal adhesions was measured *vis-à-vis* the long cell axis for flat gels and *vis-à-vis* the groove direction for topographical patterns.

2.11. Actin and tubulin intensity profiles

To obtain actin and tubulin conformity with the topographical patterns, fluorescent images of live cells expressing Lifeact-GFP and treated with SiR-tubulin were used. Intensity profiles were acquired across the cell lamellipodia using the line function in Fiji. A line 11 μm wide perpendicular to the topographical pattern was used. Single intensity profiles were individually normalized by their maximum intensity. Then, the average for several cells was computed.

2.12. Chemical treatments

To inhibit ROCK activity, 20 μM Y-27632 (Sigma-Aldrich) was added to the cell culture media. To disrupt microtubules and inhibit microtubule dynamics we added 1 μM nocodazole (Sigma-Aldrich) to the cell culture media. Drug treatments were added at least 6 h after cell seeding, were incubated for at least 6 h before measurements were performed and were maintained until the end of the experiment (see Figs. S1a and b).

2.13. Statistics

No statistical methods were used to predetermine sample size. Measurements were performed on individual cells or cell clusters (n) obtained in different independent experiments (N). The values are provided in the figure captions and in Supplementary Tables 1–15. Data presentation (as Mean value ± standard deviation (SD), Mean value ± 95% confidence interval (CI) or as Mean value ± standard error of the mean (SE)) is defined at the corresponding figure caption. Data fitting was performed using GraphPad Prism 9 to serve as an eye-guide. The statistical tests were performed using GraphPad Prism 9 and are defined at the corresponding figure caption. The p-values are specified in the figures and when they are not mentioned, differences are not statistically significant ($p > 0.05$).

3. Results

3.1. Cell elongation and alignment with topography during contact guidance change as a function of substrate rigidity

To explore the impact of substrate stiffness on topographical contact guidance, we fabricated substrates containing 2 μm wide and 1 μm deep topographical grooves and ridges made of PAA gels of different stiffness by Capillary Force Lithography [51]. We selected a stiffness range that spans from healthy tissue to grade 3 breast ductal tumor *in vivo* (3–145 kPa) [53]. Because gels swell, the spacing between ridges was slightly smaller for the PAA replicas than for the original PDMS mold used. But overall, the microfabrication technique employed was successful in providing well-defined topographies even for the softest gels (Figs. S2a and b). We then coated these grooved substrates and analogous flat, "non-patterned" counterparts, with fibronectin, that showed similar distribution in the different stiffnesses (Fig. S2c). Next, we seeded mesenchymal-like cells, NIH 3T3 fibroblasts, on them. As soon as cells started spreading on the PAA gels, they elongated and aligned to the direction of the grooves (Fig. 1b, Fig. S3a and Movie S1). This behavior corresponded to classical topographical contact guidance as found on standard PDMS grooved substrates (Fig. S3b). Next, we quantitatively characterized contact guidance associated hallmarks on cell morphology, namely cell area, elongation, and alignment with the grooves (see Methods section for details), as a function of substrate rigidity (Fig. 1c). We found cell area increasing with substrate stiffness. This trend was observed on the topographically patterned substrates (Fig. S3c), but also on flat counterparts as expected [54]. When quantifying cell elongation, we first observed that NIH 3T3 fibroblasts on flat and soft (3 kPa) PAA gels were roundish, but they broke symmetry and became spindle-like [55] when stiffness increased (Fig. 1d). This intrinsic tendency of elongate on flat substrates when stiffness increases was further enhanced by

the presence of the grooves. In this case, grooves were capable to break symmetry and induce elongation even onto soft 3 kPa substrates. Finally, while cell population showed no overall alignment (alignment index ~0) on flat substrates for any of the tested stiffnesses (Fig. 1e, see Fig. S3d for individual data points), the cells' long axis was strongly aligned with the groove's direction (alignment index ~1) for all the grooved substrates tested, independently of their rigidity (Fig. 1e). Overall, mesenchymal-like NIH 3T3 fibroblasts showed topographical contact guidance features on their morphology when cultured on grooves of different stiffness. Remarkably, these could be observed even for soft substrates (3 kPa) mimicking the physiological stiffness attributed to the ECM of soft tissues.

Supplementary data related to this article can be found at https://doi.org/10.1016/j.mtbio.2023.100593

We were then wondering if non-mesenchymal cells such as epithelial cells would also undergo topographical contact guidance on soft substrates. To address this question, we employed two different epithelial cell lines derived from breast carcinoma: MDA-MB-231 and T47D cells. Despite epithelial cells are not spindle-like naturally [56], MDA-MB-231 adopted a spindle-like morphology when sub-confluent on flat surfaces of different stiffnesses, while T47D cells showed a less elongated phenotype (Fig. S3e). These cell lines are reported to respond to topographical patterns on stiff substrates by elongating and aligning when they cannot form adherens junction (*E*-cadherin) [33]. However, their behavior onto soft patterned substrates is unknown. First, we seeded single T47D cells on stiff substrates (PDMS) and we were able to confirm cell elongation and alignment guided by the topographical patterns (Fig. S3f). Then, we seeded single MDA-MB-231 and T47D cells onto the PAA grooved gels of different stiffnesses. Spindle-like MDA-MB-231 cells behaved similar to NIH 3T3 fibroblasts (Fig. 1f and g), but T47D epithelial cells showed topographical contact guidance features in their morphology (elongation and alignment) that were heavily dependent on the stiffness of the substrate (Fig. 1f). First, even though T47D cells adhered poorly onto soft gels, when adhered, cell elongation was enhanced by the grooves in a stiffness dependent manner (Fig. 1g), breaking their natural circular shape on stiffer gels (35–145 kPa). And second, cell alignment with the direction set by the topographical pattern became stiffness dependent as well (Fig. 1h, see Fig. S2g for individual data points), being less evident on the softest gels, and in opposition to what we observed for MDA-MB-231 cells and fibroblasts. Thus, our experiments revealed that epithelial cells do experience topographical contact guidance features on soft substrates but, contrary to what we saw for the mesenchymal-like cells, cell elongation and alignment can be strongly modulated by the rigidity of the substrate when they lack a spindle-like morphology.

3.2. Cell contractility regulates contact guidance on soft topographical grooves and ridges

Bearing in mind that anisotropic contractile forces have been linked to contact guidance [33] and that the magnitude of those forces depends both on cell contractility and substrate stiffness [45,57], we next addressed the role of contractility in topographical contact guidance. We used our experimental set-up to account for the potential effects of substrate stiffness in this phenomenon combined with pharmacological treatments to reduce the contractile capability of the cells. First, given that cells such as fibroblasts can make large deformations on soft substrates [58,59], we checked if groove deformation could interfere in our experiments. Indeed, NIH 3T3 fibroblasts were able to significantly deform the topographical patterns on soft PAA gels (3–10 kPa), but not on stiffer ones (35–145 kPa) (Fig. S4a). Such deformations are typically exerted by focal adhesions, which have been shown to align with topographical patterns on stiff substrates [19,33], so we decided to characterize their distribution on the different stiffness. To do that, we used fluorescence immunostaining of paxillin and quantified focal adhesion size and alignment with the topographical grooves and ridges. Representative images showed that on grooved substrates fibroblasts developed focal adhesions localized along the direction of the grooves and ridges (Fig. 2a) while on flat surfaces they did not (Fig. S4d). Regarding the focal adhesion size, mean area increased with substrate stiffness on flat substrates but remained roughly constant on grooved substrates (Fig. 2b). Moreover, focal adhesion sizes were similar for the flat and grooved substrates when they were stiff (145 kPa), but they differed when substrates were soft (3 kPa), being significantly larger for the grooved gels. This suggests that grooves enlarged focal adhesions on soft substrates. Concerning focal adhesion alignment, the presence of the grooves led to the alignment of focal adhesions along the direction set by the topographical pattern (Fig. 2c). On the contrary, focal adhesions on flat surfaces were distributed randomly (an isotropic, non-aligned distribution would lead to 33% of the focal adhesions with $\theta_{FA} < 30°$). However, it should be noticed that since fibroblasts were naturally elongated on flat surfaces, focal adhesion could already display alignment with the defined main cell axis in the absence of any external cue. So, we analyzed focal adhesion alignment *vis-à-vis* the main cell axis direction for both flat and grooved substrates (Figs. S4b and c). On flat surfaces, ~50% of the cell focal adhesions were oriented in the direction of the cell main axis ($\theta_{FA} < 30°$) for all the substrates (Fig. 2d), confirming that focal adhesions display alignment with the defined main cell axis. For the patterned substrates, focal adhesion alignment *vis-à-vis* the main cell axis direction was enhanced compared to flat surfaces (Fig. 2d), which could be linked to the increase in cell elongation caused by the grooves (Fig. 1d). However, the percentage of FA aligned to the main cell axis on grooved substrates was 15% less than *vis-à-vis* the groove direction (Fig. 2c), where ~ 70% of focal adhesions were oriented in the direction of the grooves for all the substrates. Moreover, we observed a slight increase in focal adhesion orientation with stiffness, thus it depends weakly on the elasticity of the substrate. Altogether, focal adhesions aligned with the grooves beyond the alignment caused by the elongation of the cell in the direction of the topography. So, despite the deformations of the grooves on the softest substrates caused by cell contractility, focal adhesion elongated and aligned in the same direction of the physical restriction imposed by the topographical pattern.

It was established that focal adhesions align and mature along the groove direction, leading to the alignment of associated stress fibers, and generating anisotropic forces that translate into cell alignment on stiff substrates [33], therefore linking topographical contact guidance to cell contractility [21,28]. We have shown that focal adhesion alignment with the topographical pattern is still present on fibroblasts cultured on softer topographical patterns. So, next we pharmacologically reduced cell contractility. Decreasing NIH 3T3 fibroblasts contractility through the inhibition of the Rho-associated protein kinase (ROCK), by incubation with 20 μM Y-27632 [48,60] (Fig. S1), led to a decrease of cell elongation and alignment when cultured on PDMS grooves (Fig. S4e). We then performed an analogous set of experiments but culturing NIH 3T3 fibroblasts onto soft PAA substrates. Strikingly, a different response was observed on these materials. On the stiffest gels (35–145 kPa) cell elongation remained unchanged, but cells on the softest gels (3–10 kPa) showed an increased elongation despite fibroblast contractility was decreased (Fig. 2e and f). Such increase in elongation was mainly caused by the formation of long actin protrusions that followed the direction set by the grooves (Fig. 2e). However, this change in morphology had little impact on cell alignment, which, contrary to what was observed in PDMS substrates, was preserved (Fig. 2g, see Fig. S4f for individual data points). Although cell contractility is necessary for contact guidance on stiff substrates, initial cell elongation through contact guidance has been found to be contractility independent [22]. Then, we argued that our results on soft gels may be due to either (i) the cells becoming more elongated upon ROCK inhibition even when the topographical patterns were absent as predicted by the clutch model [57] or to (ii) being already elongated when the ROCK inhibitor was added. To clarify the first point, we evaluated cell elongation upon ROCK inhibition on flat PAA hydrogels and noticed that despite there was no statistically significant change in cell elongation (Fig. S4g), it slightly increased for soft substrates as

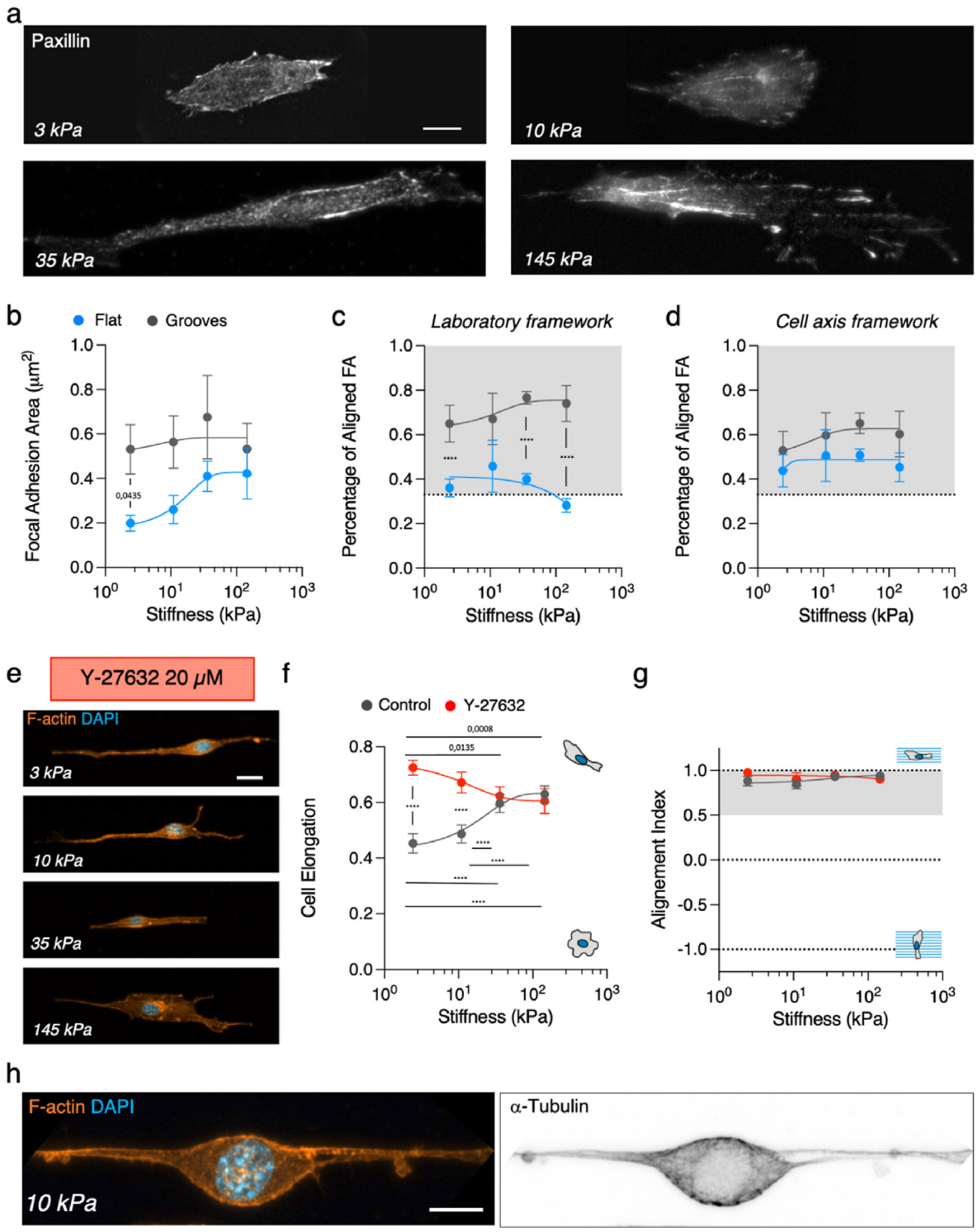

Fig. 2. Decrease of cell contractility increases contact guidance on soft topographical grooves and ridges. (**A**) Paxillin immunostaining of fibroblast on grooves of 3 kPa and 145 kPa. Examples of lamellipodial regions used for focal adhesion analysis is highlighted in yellow. Scale bar, 10 μm. (**B**) Focal adhesion area, (**C**) percentage of aligned focal adhesions as a function of increasing substrate stiffness in the laboratory framework and (**D**) percentage of aligned focal adhesions as a function of increasing substrate stiffness *vis-à-vis* the main cell axis direction. Grey area in (**C** and **D**) corresponds to values above the expected for a random distribution. N ≥ 3 experiments per condition and n ≥ 15 cells per condition. (**E**) Representative fluorescent images of 3T3 fibroblast treated with 20 μM Y-27632 on 2 μm wide grooves. Scale bar, 20 μm. (**F**) Cell elongation and (**G**) cell alignment index as a function of the substrate stiffness. N ≥ 3 experiments per condition and n ≥ 14 cells per condition. (**H**) Representative fluorescent image of the actin and tubulin cytoskeletons of 3T3 fibroblast treated with 20 μM Y-27632 on 2 μm wide grooves. Scale bar, 10 μm. See Tables S4–S5 for the exact number of cells and experiments. Data points (Mean ± SE) in (**B - D**) and in (**F**) and (**H**) were fitted as an eye-guide. Statistical significance was assessed by Tukey's tests (**F** and **G**), Welch's test (**B**) and Kruskall-Wallis' test (**C** and **D**). (For interpretation of the references to colour in this figure legend, the reader is referred to the Web version of this article.)

predicted by the clutch model. This suggests that the topographical grooves further enhance this effect. To clarify the second point, we repeated the experiments seeding cells on 3 kPa grooves already in the presence of the ROCK inhibitor. We then observed that initially roundish fibroblasts formed long protrusions emerging from opposite sides of the cell body and that these protrusions extended following the direction set by the grooves (Fig. S4h), leading to larger cell elongation than non-treated cells. Even though the inhibition of ROCK lead to a cell phenotype that may not be physiological, this result suggests that fibroblast contractility is involved in regulating contact guidance on soft gels (3–10 kPa) and that decreasing cell contractility allows cells to further elongate, thus increasing their contact guidance for these soft substrates. We then explored further these long protrusions. Immunostaining of F-actin and α-Tubulin showed that they were rich in microtubules that elongated along the topographical features (Fig. 2h). Taken all these observations together, the opposite behavior found in the response of topographical contact guidance to changes in cell contractility for soft and stiff substrates seems to indicate that cell response to topographical patterns may be mediated by different molecular actors depending on the rigidity of the substrate.

3.3. Microtubule polymerization mediates topographical contact guidance of fibroblast in a stiffness dependent manner

We found that ROCK-inhibited fibroblasts displayed long protrusions rich in microtubules along the topographical patterns. So, we wondered if microtubules may be involved in mediating the cellular response to topographical patterns for different substrate rigidities. To investigate this point, we explored the actin and tubulin distribution in fibroblast cultured on grooves of different stiffness. Our results show that F-actin structures filled in the grooves for all the substrates tested (Fig. 3a). On the contrary, microtubules, stained with α-tubulin, showed a progressive increasing conformity with the grooves and ridges when increasing the PAA substrate stiffness (Fig. 3a). Noteworthy, the α-tubulin fluorescence signal captured at the basal plane of the cells lost definition in revealing the geometry of the grooves when decreasing substrate stiffness. This effect could be linked to the pattern deformation due to cell contractility (Fig. S4a). Despite this deformation, when averaging actin intensity profiles across several cell lamellipodia *vis-à-vis* the grooves, we observed actin conformity with them for all the PAA gels (Fig. 3b and c). Strikingly, tubulin intensity profiles showed that in-groove microtubule signal exhibited no conformity with topography on 3 kPa substrates, while it was evident on $>$ 35 kPa substrates (Fig. 3d). This behavior of the microtubules can be related to a stiffness-dependent microtubule acetylation which stabilizes the microtubular network [44,62]. Thus, these results point out that cell response to topographical patterns has a potential role of microtubules which is modulated depending on the stiffness of the substrate.

Next, to further investigate the involvement of microtubules when considering substrate rigidity on contact guidance-associated phenomena, we used Nocodazole 1 μM that was sufficient to depolymerize microtubules (Fig. S1 and Fig. S5a). Then, we evaluated the effects of this drug on topographical contact guidance hallmarks evidenced by cell morphology (cell area, elongation and alignment) on grooved substrates. Nocodazole treatment led to uncoordinated protrusion dynamics (Movie S2 and Fig. 3e), and while cell area was roughly maintained, cells became less elongated and lost the stiffness-dependency (Fig. 3g). Concomitantly with the decrease in cell elongation, nocodazole treatment produced a progressive misalignment between the cells and the grooves as substrate stiffness increased (Fig. 3h, see Fig. S5b for individual data points). This progressive misalignment followed the inverse trend of the progressive stiffness-dependent tubulin conformity with the grooves and ridges observed for non-treated cells. Taken together, these results point out that microtubules are indeed involved in the stiffness-dependent cell response to topographical contact guidance.

Supplementary data related to this article can be found at https://doi.org/10.1016/j.mtbio.2023.100593

Microtubule depolymerization is reported to enhance cell contractility through an increase of RhoA activity [63,64]. So, we performed immunostaining of phosphorylated myosin upon nocodazole treatment to determine whether this was the case, and we observed that its signal was indeed enhanced (Fig. S6a). Thus, results described above may be a convolution of microtubule depolymerization and contractility enhancement. To disentangle both effects, we used ROCK inhibition (Y-27632 treatment) to decrease cell contractility in nocodazole treated cells [65] (Figure S1 and Fig. 3f). As a result, cells were more elongated than when treated with Nocodazole alone (Fig. 3g). On the softest grooves (3 kPa), cells retained an elongation similar to non-treated (control) cells, but they progressively became less elongated than their non-treated counterpart when increasing substrate stiffness. In addition, and despite the decrease in cell elongation with the stiffness of the substrate, cells showed actin structures partially aligned with the grooves for stiffness $>$10 kPa (Fig. 3f and Fig. S6b). This shows that cells can elongate through contact guidance in the absence of microtubules on soft substrates, but that the stiffer the substrate becomes, the more the cells rely on the microtubule cytoskeleton to regulate elongation, and that it cannot be counterbalanced by the alignment of actin with the topographical pattern. These actin structures co-localized with accumulations of the focal adhesion protein paxillin (Fig. S6c). The quantitative evaluation of the focal adhesions showed that upon Nocodazole and Y-27632 treatment they were smaller and less aligned with the grooves than in non-treated (control) cells (Figs. S6d–f). This, in turn, was concomitant with a decrease of cell alignment with the grooves when increasing stiffness (Fig. 3h, see Fig. S5b for individual data points). While cells on 3 kPa and 10 kPa substrates aligned with the grooves an amount similar to non-treated cells; on stiffer substrates cell alignment was significantly diminished. Thus, taken together, these results show that microtubule polymerization mediates cell elongation and alignment by topographical contact guidance in a stiffness-dependent fashion.

3.4. Microtubules are stiffness-dependent key regulators for fibroblast effective migration by topographical contact guidance

Cell elongation and alignment such as those observed here lead to directed cell migration on stiff substrates. Therefore, we next checked if this phenomenon was also observed on grooved substrates of different rigidities. For this purpose, cell motility was tracked by time-lapse microscopy. The results obtained showed cell's trajectories taking place in a narrow spatial distribution confined along the direction axis set by the grooves for all the stiffness studied (Fig. 4a and Movie S3). We then measured the total distance covered by the cells, their net displacement, and the degree of directionality of their instantaneous movements (Fig. 4b, see Methods section for details) during 6 h of migration. The total cell migration distance increased with substrate stiffness until reaching a plateau above ~35 kPa for both flat and grooved substrates (Fig. S7). On the contrary, the net cell displacement was enhanced by the presence of the grooves and was also increased with the substrate stiffness (Fig. 4c). Additionally, in contrast to flat substrates (directionality index ~ 0), grooves set a directional cell migration (directionality index $>$0.5) for all the substrates tested (Fig. 4d). Altogether, our results show that for fibroblasts the directed cell migration associated to topographical contact guidance is effective across several orders of magnitude in substrate stiffness. Importantly, this range comprises physiologically (3 kPa of healthy mammary tissue) and pathologically (145 kPa of grade 3 breast ductal tumor) relevant stiffness values.

Supplementary data related to this article can be found at https://doi.org/10.1016/j.mtbio.2023.100593

So far, we observed that directed migration by topographical contact guidance happened independently of substrate stiffness, but we did indeed observe differences in the role of microtubules in contact

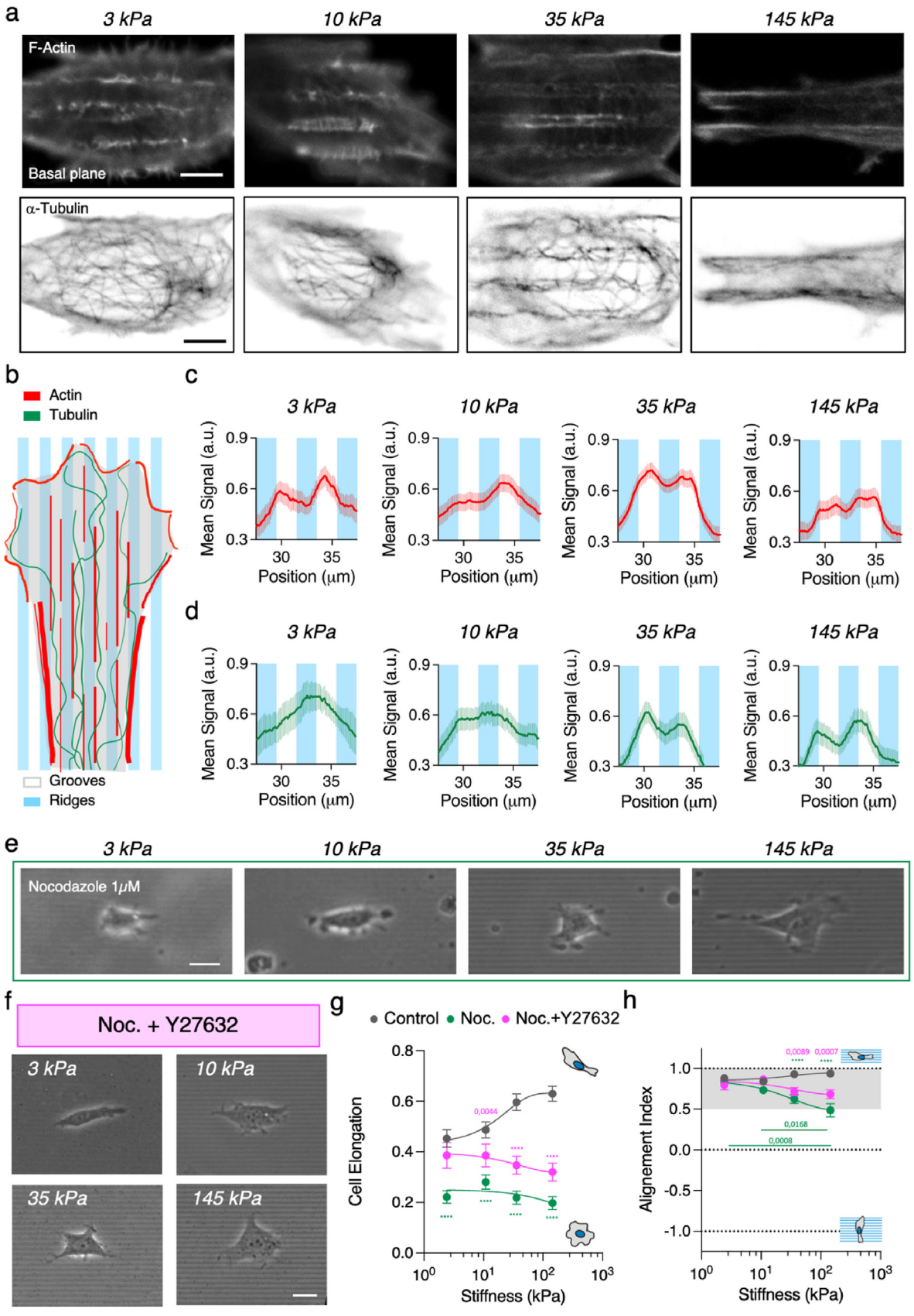

(caption on next page)

Fig. 3. Microtubule polymerization mediates NHI 3T3 fibroblasts response to topographical patterns. (**A**) F-actin (phalloidin) immunostaining of fibroblasts on grooves of increasing stiffness. Scale bar, 5 μm. a-tubulin immunostaining of fibroblasts on grooves of increasing stiffness. Scale bar, 5 μm. (**B–C**) Average intensity profile of LifeAct-GFP signal across the grooves and ridges at the lamellipodial region for increasing substrate stiffness. N ≥ 3 experiments per condition and n ≥ 28 cells per condition. Mean ± S.E. (**D**) Average intensity profile of SiR-tubulin signal across the grooves and ridges at the lamellipodial region for increasing substrate stiffness. N ≥ 3 experiments per condition and n ≥ 22 cells per condition. Mean ± S.E. (**E**) Representative phase contrast images of 3T3 fibroblast treated with 1 μM nocodazole on 2 μm wide grooves of increasing stiffness. Scale bar, 20 μm. (**F**) Representative images of 3T3 fibroblast treated with 20 μM Y-27632 and 1 μM nocodazole on 2 μm wide grooves. Scale bar, 20 μm. (**G**) Cell elongation and (**H**) cell alignment index as a function of the substrate. N ≥ 3 experiments per condition and n ≥ 15 cells per condition. See Tables S6–9 for the exact number of cells and experiments. Data points (Mean ± S.E.) in (**G**) and (**H**) were fitted as an eye-guide. Statistical significance was assessed by Tukey's tests (**H** and **G**).

guidance in a stiffness-dependent manner. Thus, we decided to explore further the cytoskeletal actors involved in directed migration through contact guidance and check whether the stiffness dependent effects of microtubule depolymerization on cell shape and alignment were also present in the directed cell migration. To do that, we tracked the movements of cells with microtubules depolymerized and increased contractility (nocodazole treatment) and with depolymerized microtubules (nocodazole and Y-27632 ROCK inhibitor treatment). Results showed that cell migration was in fact severely affected by the lack of microtubule polymerization (Fig. 4e and Figs. S8a and b). Nocodazole treatment did not greatly change cell total displacement (Fig. 4f), yet the cell net migration distance decreased drastically for all the stiffnesses studied (Fig. 4g). Upon nocodazole treatment cells experience a directional switch effect [65] that, along with uncoordinated protrusions, can lead to non-directed migration and poor net motion. Indeed, nocodazole-treated cells migrated non-directionally on 145 kPa PAA grooves (Fig. 4h). On the contrary, a less persistent but directed migration was observed on softer grooves (10–35 kPa) (Fig. 4h), evidencing that the role of microtubules is less relevant in leading to directed migration by contact guidance for soft substrates and, thus, suggesting that substrate stiffness modulates the contribution of the cytoskeletal players to the contact guidance outcome. On the other hand, when the increase in contractility caused by nocodazole treatment was reverted with ROCK inhibitor, cell migration was significantly reduced both in terms of total displacement and net distance for all the substrates tested (Fig. 4f,g and Fig. S8b). Moreover, directionality was now further decreased compared to nocodazole-treated cells (Fig. 4h), although in both cases was still higher than the one observed on flat substrates (Fig. S8c). In the case of the inhibition of both cell contractility and tubulin polymerization, it led to the loss of directional migration when compared to non-treated cells for soft (3 kPa), intermediate (35 kPa) and stiff (145 kPa) substrates (Fig. 4h). Despite the loss in directionality for 3 kPa could be attributed to the decrease in overall displacement, on stiffer substrates the loss of directionality can be linked to actual random motion (Fig. 4e). Bearing that ROCK inhibition alone did not alter cell directionality (Fig. S9), the effects observed on contact guidance can be attributed to tubulin polymerization. Altogether, these results suggest that, even though directed migration induced by contact guidance takes place for all the range of substrate stiffness in fibroblasts, it involves multiple cytoskeletal actors whose relative contributions may change with stiffness, with microtubules becoming more relevant as substrate rigidity increases.

3.5. Epithelial carcinoma cells perform directed migration induced by contact guidance in a stiffness dependent manner

Up to this point, our experiments revealed that mesenchymal-like cells experienced topographical contact guidance and directed cell migration regardless the stiffness of the substrate, even if complex stiffness-dependent mechanisms are involved in the process. Moreover, we also saw that epithelial cells also experienced topographically induced elongation and alignment, but this was strongly dependent on the substrate stiffness and the spindle-like morphology of the cells. Therefore, we wondered if for epithelial cells the substrate stiffness affected directed cell migration. To check this, we seeded T47D carcinoma cells at low density and the motility of individual cells was tracked by time-lapse microscopy (Movie S4). In agreement with previous experiments [33], on stiff PDMS substrates T47D cells also experienced weak directed migration by contact guidance and their trajectories were much shorter than the ones observed for 3T3 fibroblasts (Fig. S10). Noteworthy, when T47D epithelial cells were cultured on softer substrates (approaching physiological and pathological values of soft tissues), single cell trajectories were significantly affected by the grooves rigidity and differed greatly from substrates with non-physiological stiffness values. Specifically, cell trajectories were longer and became more restricted to the direction set by the grooves than on stiff PDMS (Fig. 5a, Movie S5). In addition, total cell displacement, net distance, and directionality index increased when topographical patterns became stiffer (up to 145 kPa). Basically, these parameters showed that directed migration by contact guidance for T47D cells had a non-monotonic behavior with the substrate stiffness within the range tested (Fig. 5b–d and Fig. S10), being increasingly effective for cells cultured on physiological stiffness but decreasing for cells cultured on non-physiological ones. Remarkably, in here we have found that non-migratory T47D cells can develop a stiffness-dependent migratory phenotype when cultured on topographical grooves with rigidities similar to the ones encountered on soft tissues, highlighting the relevance of including the physiological values of the matrix when addressing topographical contact guidance for this cell type.

Supplementary data related to this article can be found at https://doi.org/10.1016/j.mtbio.2023.100593

Epithelial cells form focal adhesions that tend to be small, their microtubules are organized in setting cell apical-basal polarity, and they do not migrate directionally as single cells in physiological conditions [56]. We then wondered if these differences between epithelial and mesenchymal-like cells together with the ones described above, namely stiffness-dependent and stiffness-independent contact guidance, would link to differences in the actors involved in contact guidance for epithelial cells. So, we treated T47D epithelial cells cultured on 35 kPa and 145 kPa substrates with the same inhibitors used for NIH3T3 fibroblasts. Decrease in cell contractility by ROCK inhibition had little impact in cell directionality (Fig. 5e and f). Despite trajectories were shorter than for non-treated cells (Figs. S11a and b), T47D cells migrated following the direction set by the grooves, similar to what was observed for fibroblasts (Fig. S9). Upon nocodazole treatment, total and net distances decreased (Fig. 5g and Fig. S11c) and the directionality of cells' trajectories was significantly reduced as well (Fig. 5h). As for NIH3T3, this loss of directionality was the convoluted effect of microtubule depolymerization and increased contractility. To disentangle these two effects, we added Y-27632. Contrary to what we observed for NIH3T3 fibroblasts, inhibition of both ROCK activity and tubulin polymerization led to an increase of cells' directionality compared to nocodazole treatment (Fig. 5h). This result suggests that T47D epithelial cells treated with nocodazole performed less directional movement because of increased contractility, rather than because of lacking microtubules. So, while tubulin polymerization is needed for directional migration in fibroblasts on 35–145 kPa grooves, it is dispensable in the case of T47D epithelial cells.

Next, we compared T47D migration to MDA-MB-231. While both are breast cancer epithelial cell lines, MDA-MB-231 have a spindle-like morphology similar to fibroblasts. Also, they are reported to be more migratory than T47D cells on stiffer topographies [33]. We tracked

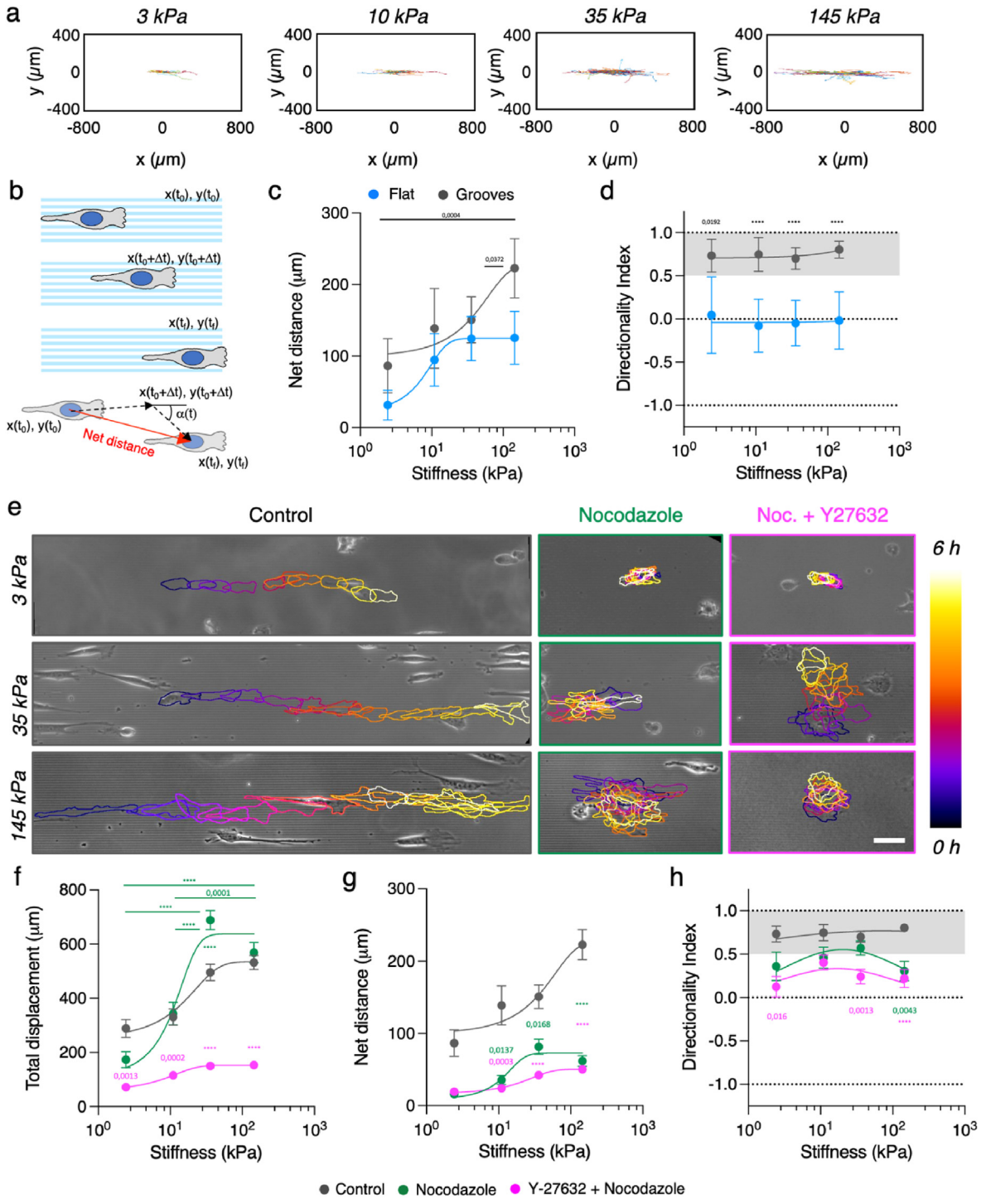

Fig. 4. Microtubule depolymerization leads to a stiffness dependent topographically guided migration. (**A**) Single cell trajectories on grooved hydrogels of different stiffness. N ≥ 3 experiments per condition and n ≥ 13 cells per condition. (**B**) Scheme depicting the quantification of cell trajectories. (**C**) Cells' net distances versus substrate stiffness. (**D**) Trajectory directionality as a function of substrate stiffness. (**E**) Cell trajectories on grooves of different stiffness for control cells, cells treated with nocodazole (N ≥ 3 experiments per condition and n ≥ 11 cells per condition) and cells treated with Y-27632 and nocodazole (N ≥ 2 experiments per condition and n ≥ 10 cells per condition). Cell outlines are color-coded by time. Scale bar, 50 μm. (**F**) Total displacement, (**G**) net distance and (**H**) trajectory directionality index of cells treated with nocodazole or Y-27632 and nocodazole. See Tables S11–S13 for the number of cells and experiments. Data points (Mean ± SE) in (**C**), (**D**), and (**F**–**H**) were fitted as an eye-guide. Statistical significance was assessed by Tukey's tests. (For interpretation of the references to colour in this figure legend, the reader is referred to the Web version of this article.)

MDA-MB-231 cells on topographical grooves for 6 h (Fig. S12a). When computing total displacement (Fig. S12b), net distance (Fig. S12c) and directionality index (Fig. S12d), we found that MDA-MB-231 cells performed contact guidance in a stiffness dependent manner, similar to T47D cells. However, efficiency in directed migration of MDA-MB-231 cells was higher than T47D on 35–145 kPa substrates, and closer to NIH

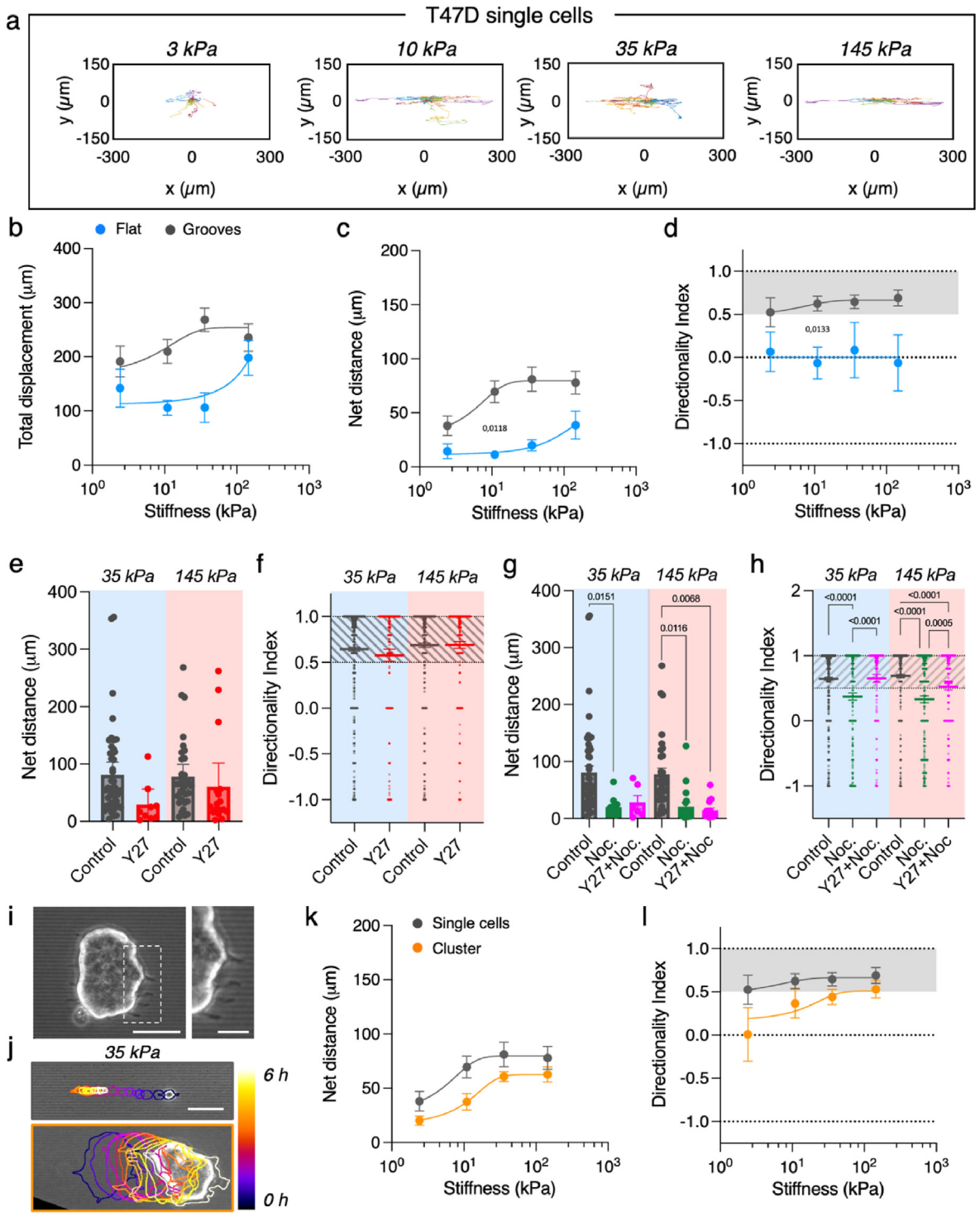

Fig. 5. T47D carcinoma cells perform directed migration as a function of stiffness. (**A**) Single T47D cells' trajectories on grooves of increasing stiffness. (**B**) Total displacement, (**C**) net distance and (**D**) trajectory directionality index of single T47D cells migrating on flat and grooved polyacrylamide hydrogels of increasing stiffness. N ≥ 3 experiments per condition and n ≥ 14 cells per condition. (**E**) Net distance and (**F**) trajectory directionality index of single T47D cells treated with Y-27632 on 35 kPa and 145 kPa grooves. N ≥ 3 experiments per condition and n ≥ 9 cells per condition. (**G**) Net distance and (**H**) trajectory directionality index of single T47D cells treated with Nocodazole or Nocodazole + Y-27632 on 35 kPa and 145 kPa grooves. N ≥ 3 experiments per condition and n ≥ 6 cells per condition. (**I**) Clusters of T47D cells extend protrusions along the grooves. Scale bar, 50 μm. Inset scale bar, 20 μm. (**J**) Cell trajectories on grooves of 35 kPa for control single T47D cells and T47D cell clusters. Outlines are color-coded by time. Scale bar, 50 μm. (**K**) Net distance and (**L**) directionality as a function of groove stiffness for T47D cell clusters and single T47D cells. N ≥ 3 experiments per condition and n ≥ 7 clusters per condition. See Tables S15 and S16 for the number of cells and experiments. Data points (Mean ± SE) in (**B – D**), and (**K–L**) were fitted as an eye-guide. Data points, mean ± SE in (**E** and **G**) and Data points, mean ± CI in (**F** and **H**). Statistical significance was assessed by Tukey's tests in (**B – D**) and (**K–L**), ANOVA in (**E** and **G**), and Kruskal-Wallis in (**F** and **H**). (For interpretation of the references to colour in this figure legend, the reader is referred to the Web version of this article.)

3T3 fibroblasts. Thus, in terms of contact guidance, MDA-MB-231 cells behave as epithelial cells on soft topographical grooves (3–10 kPa) but as spindle-like cells on stiffer ones (35–145 kPa).

Finally, we found that T47D epithelial cells formed clusters (Fig. 5i) that allowed us to investigate directed collective migration by contact guidance and its dependence on the stiffness of the substrate. These 2D cell clusters, which were becoming more 3D-like as the substrate softened (Fig. S13a), displayed sizes between 3000 and 8000 μm^2 (Fig. S13b). When in the presence of topographical patterns, we observed that T47D clusters formed cell protrusions along the grooves' direction (Fig. 5i inset) and in some cases performed directed migration (Fig. 5j, and Movie S6). Similar to single cells, T47D clusters barely migrated on PDMS topographical patterns, and their movement was close to random (Fig. S13c). However, when seeded on softer topographical patterns, they did show a larger motility (Fig. S13d). Again, a non-monotonous trend with the substrate stiffness was observed for the effective migration of the clusters and their net distance (Fig. 5k,l and Fig. S13c). On soft 3 kPa grooves, clusters were weakly adhered and performed fluctuant motions, resulting in random migration (Movie S7). Then, this migration became progressively more directed when the stiffness of the underlying substrate increased (Fig. 5l). Taking these data together, we observed that epithelial cells both as single cells and as cell clusters perform directional and efficient migration triggered by topographical contact guidance when they are presented with substrates that possess stiffness values within the range of soft tissues.

Supplementary data related to this article can be found at https://doi.org/10.1016/j.mtbio.2023.100593

4. Discussion

Contact guidance has been known for more than a century [66], but the key aspects of how cells sense the underlaying topographical patterns and how the cytoskeletal elements contribute to this phenomenon have started to be clarified only in recent years and are being still scrutinized [33,34,67,68]. Mechanics plays a central role in the behavior of the cellular structures involved in sensing contact guidance, but the mechanical properties of the substrates have been completely overlooked when studying this phenomenon. Only recent developments in microfabrication techniques have allowed to pattern soft gels [51,69] and study contact guidance in the range of stiffness relevant for soft tissues. For example, T-cells perform topographically induced contact guidance only onto soft grooves (16 kPa) [49]. In here we show that the stiffness of

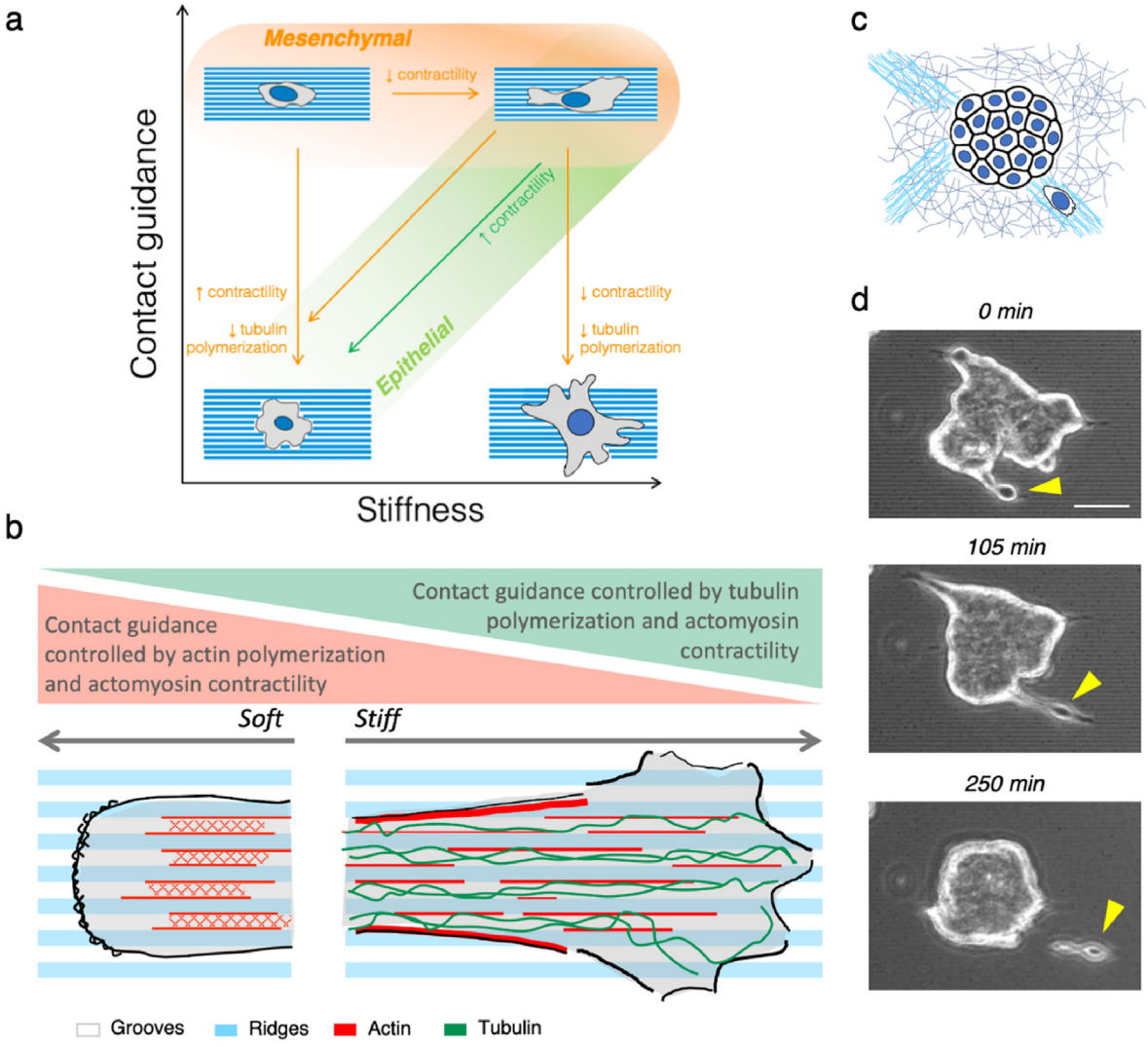

Fig. 6. (**A**) Schematics of the proposed contact guidance response to changes in substrate stiffness. Mesenchymal-like cells perform contact guidance independently of substrate stiffness while epithelial cells perform contact guidance as a function of substrate stiffness. (**B**) Schematics of the different cytoskeletal components involved in contact guidance. (**C**) Scheme of a cluster of T47D cells and single T47D cells navigating on aligned extracellular matrix fibers. (**D**) Snapshots of a T47D cell detaching from the periphery of a cell cluster.

the topographical patterns modulates the contact guidance response of fibroblasts and epithelial cells (Fig. 1). Grooves enhance the elongation of spindle-like fibroblasts across all the stiffness range, being the highest impact observed on soft substrates (3 kPa). On the contrary, grooves can break symmetry and elongate epithelial cells, which do not typically have spindle shape, when the substrate stiffens (35–145 kPa) (Fig. 6a).

These changes in contact guidance as a function of the rigidity of the topographical grooves involve several cytoskeletal actors. While focal adhesion alignment and actin conformity with the topographical shapes were observed for all the stiffness range (Figs. 2c and 3a,c), the response of the microtubule cytoskeleton to the topographical pattern was stiffness-dependent (Fig. 3a,d). Further inhibition of tubulin polymerization in fibroblasts showed that the loss of both cell alignment and directional migration increased with substrate stiffening (Figs. 3h and 4h). On the contrary, cell elongation and alignment to the grooves were invariant to tubulin depolymerization on soft substrates but were sensitive to changes in contractility (Figs. 2f and 3g). These results suggest that there is a balance between cell contractility and tubulin polymerization in regulating fibroblasts response to topographical grooves. On soft patterns actin polymerization and actomyosin contractility seem to be the main drivers of contact guidance, while on stiff substrates tubulin conformity to the patterns becomes more prominent (Fig. 6b). This dual source of the topographical response leads to the stiffness-independent contact guidance observed in fibroblasts. Interestingly, tubulin polymerization doesn't seem to be as prominent in contact guidance response for epithelial cells (Fig. 5h), which leads to the observed stiffness-dependent response to the topographical grooves (Fig. 1h,l and Fig. 5c,d,l). Furthermore, when both actomyosin contractility and tubulin polymerization were inhibited, this hindered the ability of the focal adhesions to align with the grooves and ridges in fibroblasts. Whether this effect was due to a lack of cell contractility [33] or to the role of microtubules in the dynamics of focal adhesion complexes during mechanosensation [44,64,70] remains an open question. Moreover, the interaction of the cell membrane with the edges of the topographical structures on soft substrates should be further addressed, since it has been shown key in contact guidance [68,71].

In a previous study, perturbation of the microtubule-contractility axis regulated T-cell contact guidance when groove elasticity changed [49]. Here, we show that in the case of fibroblasts, actomyosin contractility regulates contact guidance on soft substrates as well, but microtubules take over in being the major regulator of contact guidance when the substrate stiffens. This translated into a stiffness independent contact guidance migration for fibroblasts, which was reported for T-cells only when Rho-A activity was increased through tubulin depolymerization. Remarkably, we show that epithelial cells have the opposite response when contractility was increased and contact guidance was stopped. This highlights the importance of the cell phenotype (and the associated cytoskeleton organization) on experiencing contact guidance. Indeed, in breast carcinoma epithelial cells, substrate stiffness modulated the cell's response to the topographical patterns in a third manner: contact guidance increases as the groove rigidity increases (Figs. 1 and 5). Unlike fibroblasts, epithelial cells have small focal adhesions and apico-basal polarized microtubule networks [56], so the interaction between adhesions, actomyosin and microtubules unfolds with stiffness differently than for fibroblasts, and tubulin polymerization is less important. Stiffness-dependent contact guidance was even more dramatic when cell-cell adhesions were involved. Epithelial clusters barely moved on PDMS, but when substrate stiffness was decreased to more physiological values, they migrated collectively in the direction of the grooves. This behavior was again abrogated when the stiffness was further decreased. Interestingly, a stiffness dependent migration behavior of epithelial clusters similar to the one we found has been recently reported on flat stiffness gradients [72]. In our experiments, topographical patterns with intermediate stiffness (~35 kPa) could be viewed as stiff and aligned protein fibers of the tumoral stroma (Fig. 6c). Cells at the periphery of tumor cell clusters may use these stiff aligned fibers to adhere, align and migrate outwards, detaching from the cluster (Fig. 6d). This shows that both matrix stiffening [73] and alignment of extracellular matrix fibers [10] could synergize during metastasis and cancer cell invasion. Moreover, as we showed stiffness-dependent contact guidance was also observed for cell clusters, so not only single cells but cell clusters could take advantage of aligned and stiff fibers during the process of invasion.

5. Conclusion

Together, our findings demonstrated that substrate stiffness mediates cell response to topographical grooves. We showed that mesenchymal-like cells rely on different cytoskeletal actors to mediate their response to their environment's architecture depending on substrate stiffness. Actomyosin contractility on soft grooves and tubulin polymerization on stiff ones cooperate to produce a stiffness independent output to contact guidance. Moreover, we demonstrated that an increase in groove stiffness enhanced directional response of epithelial cells in a biphasic fashion. And that epithelial-like cells experience stiffness dependent contact guidance even as multicellular clusters, where cell-cell adhesions are involved. Therefore, only acknowledging substrate stiffness when studying the effects of topography in cell behavior, we will be able to fully comprehend how cells respond to anisotropic matrix architectures *in vivo*.

Credit author statement

Jordi Comelles: Conceptualization, Methodology, Investigation, Validation, Formal Analysis, Visualization, Supervision, Writing—original draft, Writing—review & editing, Project administration. Vanessa Fernández-Majada: Investigation and Writing—review & editing. Verónica Acevedo: Investigation and Writing—review & editing. Beatriz Rebollo-Calderón: Investigation and Writing—review & editing. Elena Martínez: Conceptualization, Supervision, Writing—original draft, Writing—review & editing, Project administration, Funding acquisition.

Declaration of competing interest

The authors declare that they have no known competing financial interests or personal relationships that could have appeared to influence the work reported in this paper.

Data availability

Data will be made available on request.

Acknowledgements

We thank the Martinez Lab members and P. Roca-Cusachs for discussions and help, and A.L. Godeau and R. Sunyer for critical reading of the manuscript.Funding for this project was provided by.European Union Horizon 2020 ERCgrant (agreement no. 647863 - COMIET).CERCA Programme/Generalitat de Catalunya (2017-SGR-1079).Spanish Ministry of Economy and Competitiveness (TEC2017-83716-C2-1-R, and the Severo Ochoa Programme for Centres of Excellence in R&D 2016–2019).The results presented here only reflect the views of the authors; the European Commission is not responsible for any use that may be made of the information it contains.

Appendix A. Supplementary data

Supplementary data to this article can be found online at https://doi.org/10.1016/j.mtbio.2023.100593.

References

[1] V. Lecaudey, G. Cakan-Akdogan, W.H.J. Norton, D. Gilmour, Dynamic Fgf signaling couples morphogenesis and migration in the zebrafish lateral line primordium, Development (Cambridge, U. K.) 135 (2008) 2695–2705, https://doi.org/10.1242/dev.025981.

[2] F. Calvo, N. Ege, A. Grande-Garcia, S. Hooper, R.P. Jenkins, S.I. Chaudhry, K. Harrington, P. Williamson, E. Moeendarbary, G. Charras, E. Sahai, Mechanotransduction and YAP-dependent matrix remodelling is required for the generation and maintenance of cancer-associated fibroblasts, Nat. Cell Biol. 15 (2013) 637–646, https://doi.org/10.1038/ncb2756.

[3] M. Weber, R. Hauschild, J. Schwarz, C. Moussion, I. de Vries, D.F. Legler, S. a Luther, T. Bollenbach, M. Sixt, Interstitial dendritic cell guidance by haptotactic chemokine gradients, Science 339 (2013) 328–332, https://doi.org/10.1126/science.1228456.

[4] R. Sunyer, V. Conte, J. Escribano, A. Elosegui-Artola, A. Labernadie, L. Valon, D. Navajas, J.M. García-Aznar, P. Roca-Cusachs, X. Trepat, J.J. Munoz, Collective cell durotaxis emerges from long-range intercellular force transmission, Science 353 (2016) 1157–1161, https://doi.org/10.5061/dryad.r8h3n.

[5] A. Shellard, R. Mayor, All roads lead to directional cell migration, Trends Cell Biol. 30 (2020) 852–868, https://doi.org/10.1016/j.tcb.2020.08.002.

[6] S. SenGupta, C.A. Parent, J.E. Bear, The principles of directed cell migration, Nat. Rev. Mol. Cell Biol. 22 (2021) 529–547, https://doi.org/10.1038/s41580-021-00366-6.

[7] N. Nakatsuji, K.E. Johnson, Experimental manipulation of a contact guidance system in amphibian gastrulation by mechanical tension, Nature 307 (1984) 453–455.

[8] S. Dekoninck, E. Hannezo, A. Sifrim, Y.A. Miroshnikova, M. Aragona, M. Malfait, S. Gargouri, C. de Neunheuser, C. Dubois, T. Voet, S.A. Wickström, B.D. Simons, C. Blanpain, Defining the design principles of skin epidermis postnatal growth, Cell 181 (2020) 604–620.e22, https://doi.org/10.1016/j.cell.2020.03.015.

[9] P.P. Provenzano, K.W. Eliceiri, J.M. Campbell, D.R. Inman, J.G. White, P.J. Keely, Collagen reorganization at the tumor-stromal interface facilitates local invasion, BMC Med. 4 (2006) 38, https://doi.org/10.1186/1741-7015-4-38.

[10] C.R. Drifka, A.G. Loeffler, K. Mathewson, A. Keikhosravi, J.C. Eickhoff, Y. Liu, S.M. Weber, W. John Kao, K.W. Eliceiri, Highly aligned stromal collagen is a negative prognostic factor following pancreatic ductal adenocarcinoma resection, Oncotarget 7 (2016) 76197–76213, https://doi.org/10.18632/oncotarget.12772.

[11] A. Ray, M.K. Callaway, N.J. Rodríguez-Merced, A.L. Crampton, M. Carlson, K.B. Emme, E.A. Ensminger, A.A. Kinne, J.H. Schrope, H.R. Rasmussen, H. Jiang, D.G. DeNardo, D.K. Wood, P.P. Provenzano, Stromal architecture directs early dissemination in pancreatic ductal adenocarcinoma, JCI Insight 7 (2022), e150330, https://doi.org/10.1172/jci.insight.150330.

[12] P. Clark, P. Connolly, A.S.G. Curtis, J.A.T. Dow, C.D.W. Wilkinson, Topographical Control of Cell Behavior: II. Multiple Grooved Substrata, Development 108 (1990) 635–644.

[13] C. Oakley, D.M. Brunette, The sequence of alignment of microtubules, focal contacts and actin filaments in fibroblasts spreading on smooth and grooved titanium substrata, J. Cell Sci. 106 (Pt 1) (1993) 343–354.

[14] C. Oakley, N.A. Jaeger, D.M. Brunette, Sensitivity of fibroblasts and their cytoskeletons to substratum topographies: topographic guidance and topographic compensation by micromachined grooves of different dimensions, Exp. Cell Res. 234 (1997) 413–424, https://doi.org/10.1006/excr.1997.3625.

[15] X.F. Walboomers, L.A. Ginsel, J.A. Jansen, Early spreading events of fibroblasts on microgrooved substrates, J. Biomed. Mater. Res. 51 (2000) 529–534, https://doi.org/10.1002/1097-4636(20000905)51:3<529::AID-JBM30>3.0.CO;2-R.

[16] P.M. Stevenson, A.M. Donald, Identification of three regimes of behavior for cell attachment on topographically patterned substrates, Langmuir 25 (2009) 367–376.

[17] S. Al-Haque, J.W. Miklas, N. Feric, L.L.Y. Chiu, W.L.K. Chen, C.A. Simmons, M. Radisic, Hydrogel substrate stiffness and topography interact to induce contact guidance in cardiac fibroblasts, Macromol. Biosci. 12 (2012) 1342–1353, https://doi.org/10.1002/mabi.201200042.

[18] C. Londono, M.J. Loureiro, B. Slater, P.B. Lücker, J. Soleas, S. Sathananthan, J.S. Aitchison, A.J. Kabla, A.P. McGuigan, Nonautonomous contact guidance signaling during collective cell migration, Proc. Natl. Acad. Sci. U.S.A. 111 (2014) 1807–1812, https://doi.org/10.1073/pnas.1321852111.

[19] A.I. Teixeira, G.A. Abrams, P.J. Bertics, C.J. Murphy, P.F. Nealey, Epithelial contact guidance on well-defined micro- and nanostructured substrates, J. Cell Sci. 116 (2003) 1881–1892, https://doi.org/10.1242/jcs.00383.

[20] B. Dreier, V.K. Raghunathan, P. Russell, C.J. Murphy, Focal adhesion kinase knockdown modulates the response of human corneal epithelial cells to topographic cues, Acta Biomater. 8 (2012) 4285–4294, https://doi.org/10.1016/j.actbio.2012.07.004.

[21] D. Franco, M. Klingauf, M. Bednarzik, M. Cecchini, V. Kurtcuoglu, J. Gobrecht, D. Poulikakos, A. Ferrari, Control of initial endothelial spreading by topographic activation of focal adhesion kinase, Soft Matter 7 (2011) 7313–7324, https://doi.org/10.1039/c1sm05191a.

[22] A. Sales Ramos, A. Holle, R. Kemkemer, Initial contact guidance during cell spreading is contractility-independent, Soft Matter 13 (2017) 5158–5167, https://doi.org/10.1039/C6SM02685K.

[23] A. Rajnicek, C. McCaig, Guidance of CNS growth cones by substratum grooves and ridges: effects of inhibitors of the cytoskeleton, calcium channels and signal transduction pathways, J. Cell Sci. 110 (1997) 2915–2924.

[24] I. Tonazzini, S. Meucci, P. Faraci, F. Beltram, M. Cecchini, Neuronal differentiation on anisotropic substrates and the influence of nanotopographical noise on neurite contact guidance, Biomaterials 34 (2013) 6027–6036, https://doi.org/10.1016/j.biomaterials.2013.04.039.

[25] J. Mai, C. Sun, S. Li, X. Zhang, A microfabricated platform probing cytoskeleton dynamics using multidirectional topographical cues, Biomed. Microdevices 9 (2007) 523–531, https://doi.org/10.1007/s10544-007-9060-8.

[26] A.C. Saito, T.S. Matsui, T. Ohishi, M. Sato, S. Deguchi, Contact guidance of smooth muscle cells is associated with tension-mediated adhesion maturation, Exp. Cell Res. 327 (2014) 1–11, https://doi.org/10.1016/j.yexcr.2014.05.002.

[27] S. Gerecht, C.J. Bettinger, Z. Zhang, J.T. Borenstein, G. Vunjak-Novakovic, R. Langer, The effect of actin disrupting agents on contact guidance of human embryonic stem cells, Biomaterials 28 (2007) 4068–4077, https://doi.org/10.1016/j.biomaterials.2007.05.027.

[28] A. Calzado-Martin, A. Mendez-Vilas, M. Multigner, L. Saldaña, J.L. Gonzalez-Carrasco, M.L. Gonzalez-Martin, N. Vilaboa, On the role of RhoA/ROCK signaling in contact guidance of bone-forming cells on anisotropic Ti6Al4V surfaces, Acta Biomater. 7 (2011) 1890–1901, https://doi.org/10.1016/j.actbio.2010.11.035.

[29] M.J. Dalby, A. Hart, S.J. Yarwood, The effect of the RACK1 signalling protein on the regulation of cell adhesion and cell contact guidance on nanometric grooves, Biomaterials 29 (2008) 282–289, https://doi.org/10.1016/j.biomaterials.2007.09.030.

[30] J. Wang, J.W. Petefish, A.C. Hillier, I.C. Schneider, Epitaxially grown collagen fibrils reveal diversity in contact guidance behavior among cancer cells, Langmuir 31 (2015) 307–314, https://doi.org/10.1021/la503254x.

[31] C.D. Paul, D.J. Shea, M.R. Mahoney, A. Chai, V. Laney, W.-C. Hung, K. Konstantopoulos, Interplay of the physical microenvironment, contact guidance, and intracellular signaling in cell decision making, Faseb. J. 30 (2016) 2161–2170, https://doi.org/10.1096/fj.201500199R.

[32] J. Wang, I.C. Schneider, Myosin phosphorylation on stress fibers predicts contact guidance behavior across diverse breast cancer cells, Biomaterials 120 (2017) 81–93, https://doi.org/10.1016/j.biomaterials.2016.11.035.

[33] A. Ray, O. Lee, Z. Win, R.M. Edwards, P.W. Alford, D.-H. Kim, P.P. Provenzano, Anisotropic forces from spatially constrained focal adhesions mediate contact guidance directed cell migration, Nat. Commun. 8 (2017), 14923, https://doi.org/10.1038/ncomms14923.

[34] E.D. Tabdanov, V. Puram, A. Zhovmer, P.P. Provenzano, Microtubule-actomyosin mechanical cooperation during contact guidance sensing, Cell Rep. 25 (2018) 328–337.e6, https://doi.org/10.1016/j.celrep.2018.09.030.

[35] D.W. Hamilton, C. Oakley, N.A.F. Jaeger, D.M. Brunette, Directional change produced by perpendicularly-oriented microgrooves is microtubule-dependent for fibroblasts and epithelium, Cell Motil Cytoskeleton 66 (2009) 260–271, https://doi.org/10.1002/cm.20354.

[36] K. Lee, E.H. Kim, N. Oh, N.A. Tuan, N.H. Bae, S.J. Lee, K.G. Lee, C.-Y. Eom, E.K. Yim, S. Park, Contribution of actin filaments and microtubules to cell elongation and alignment depends on the grating depth of microgratings, J. Nanobiotechnol. 14 (2016) 35, https://doi.org/10.1186/s12951-016-0187-8.

[37] A. Ferrari, M. Cecchini, M. Serresi, P. Faraci, D. Pisignano, F. Beltram, Neuronal polarity selection by topography-induced focal adhesion control, Biomaterials 31 (2010) 4682–4694, https://doi.org/10.1016/j.biomaterials.2010.02.032.

[38] J. Swift, I.L. Ivanovska, A. Buxboim, T. Harada, P.C.D.P. Dingal, J. Pinter, J.D. Pajerowski, K.R. Spinler, J.-W. Shin, M. Tewari, F. Rehfeldt, D.W. Speicher, Dennis E. Discher, Nucler Lamin-A scales with tissue stiffness and enhances matrix-directed differentiation, Science 341 (2013), 1240104, https://doi.org/10.1126/science.1243643.

[39] Y. Shen, X. Wang, J. Lu, M. Salfenmoser, N.M. Wirsik, N. Schleussner, A. Imle, A. Freire Valls, P. Radhakrishnan, J. Liang, G. Wang, T. Muley, M. Schneider, C. Ruiz de Almodovar, A. Diz-Muñoz, T. Schmidt, Reduction of liver metastasis stiffness improves response to bevacizumab in metastatic colorectal cancer, Cancer Cell 37 (2020) 800–817.e7, https://doi.org/10.1016/j.ccell.2020.05.005.

[40] T. Yeung, P.C. Georges, L.A. Flanagan, B. Marg, M. Ortiz, M. Funaki, N. Zahir, W. Ming, V. Weaver, P.A. Janmey, Effects of substrate stiffness on cell morphology, cytoskeletal structure, and adhesion, Cell Motil Cytoskeleton 60 (2005) 24–34, https://doi.org/10.1002/cm.20041.

[41] A. Engler, M. Sheehan, H.L. Sweeney, D.E. Discher, Substrate compliance vs ligand density in cell on gel responses, Biophys. J. 86 (2004) 617–628, https://doi.org/10.1016/S0006-3495(04)74140-5.

[42] W.H. Guo, M.T. Frey, N.A. Burnham, Y.L. Wang, Substrate rigidity regulates the formation and maintenance of tissues, Biophys. J. 90 (2006) 2213–2220, https://doi.org/10.1529/biophysj.105.070144.

[43] J. Solon, I. Levental, K. Sengupta, P.C. Georges, P.A. Janmey, Fibroblast adaptation and stiffness matching to soft elastic substrates, Biophys. J. 93 (2007) 4453–4461, https://doi.org/10.1529/biophysj.106.101386.

[44] S. Seetharaman, B. Vianay, V. Roca, A.J. Farrugia, C. De Pascalis, B. Boëda, F. Dingli, D. Loew, S. Vassilopoulos, A.D. Bershadsky, M. Théry, S. Etienne-Manneville, Microtubules tune mechanosensitive cell responses, Nat. Mater. 21 (2022) 366–377, https://doi.org/10.1101/2020.07.22.205203.

[45] A. Elosegui-Artola, R. Oria, Y. Chen, A. Kosmalska, C. Pérez-González, N. Castro, C. Zhu, X. Trepat, P. Roca-Cusachs, Mechanical regulation of a molecular clutch defines force transmission and transduction in response to matrix rigidity, Nat. Cell Biol. 18 (2016) 540–548, https://doi.org/10.1038/ncb3336.

[46] D.T. Butcher, T. Alliston, V.M. Weaver, A tense situation: forcing tumour progression, Nat. Rev. Cancer 9 (2009) 108–122, https://doi.org/10.1038/nrc2544.

[47] P. Lu, V.M. Weaver, Z. Werb, The extracellular matrix: a dynamic niche in cancer progression, JCB (J. Cell Biol.) 196 (2012) 395–406, https://doi.org/10.1083/jcb.201102147.

[48] D. Caballero, L. Palacios, P.P. Freitas, J. Samitier, An interplay between matrix anisotropy and actomyosin contractility regulates 3D-directed cell migration, Adv. Funct. Mater. 27 (2017), 1702322, https://doi.org/10.1002/adfm.201702322.
[49] E.D. Tabdanov, N.J. Rodríguez-Merced, A.X. Cartagena-Rivera, V.V. Puram, M.K. Callaway, E.A. Ensminger, E.J. Pomeroy, K. Yamamoto, W.S. Lahr, B.R. Webber, B.S. Moriarity, A.S. Zhovmer, P.P. Provenzano, Engineering T cells to enhance 3D migration through structurally and mechanically complex tumor microenvironments, Nat. Commun. 12 (2021) 2815, https://doi.org/10.1038/s41467-021-22985-5.
[50] T.G. Oyama, K. Oyama, A. Kimura, F. Yoshida, R. Ishida, M. Yamazaki, H. Miyoshi, M. Taguchi, Collagen hydrogels with controllable combined cues of elasticity and topography to regulate cellular processes, Biomed. Mater. 16 (2021), 45037, https://doi.org/10.1088/1748-605x/ac0452.
[51] J. Comelles, V. Fernández-Majada, N.N. Berlanga-Navarro, V. Acevedo, K. Paszkowska, E. Martínez, Microfabrication of poly(acrylamide) hydrogels with independently controlled topography and stiffness, Biofabrication 12 (2020), 025023, https://doi.org/10.1088/1758-5090/ab7552.
[52] S.V. Plotnikov, B. Sabass, U.S. Schwarz, C.M. Waterman, High-Resolution Traction Force Microscopy, Methods Cell Biol. 123 (2014) 367–394, https://doi.org/10.1016/B978-0-12-420138-5.00020-3.
[53] S.J.P. Pratt, R.M. Lee, S.S. Martin, The mechanical microenvironment in breast cancer, Cancers 12 (2020) 1452, https://doi.org/10.3390/cancers12061452.
[54] R. Sunyer, A.J. Jin, R. Nossal, D.L. Sackett, Fabrication of hydrogels with steep stiffness gradients for studying cell mechanical response, PLoS One 7 (2012) e46107, https://doi.org/10.1371/journal.pone.0046107.
[55] S. Etienne-Manneville, Actin and microtubules in cell motility: which one is in control? Traffic 5 (2004) 470–477, https://doi.org/10.1111/j.1600-0854.2004.00196.x.
[56] A. Müsch, Microtubule organization and function in epithelial cells, Traffic 5 (2004) 1–9, https://doi.org/10.1111/j.1600-0854.2003.00149.x.
[57] B.L. Bangasser, G.A. Shamsan, C.E. Chan, K.N. Opoku, E. Tüzel, B.W. Schlichtmann, J.A. Kasim, B.J. Fuller, B.R. McCullough, S.S. Rosenfeld, D.J. Odde, Shifting the optimal stiffness for cell migration, Nat. Commun. 8 (2017) 15313, https://doi.org/10.1038/ncomms15313.
[58] R.J. Pelham, Y.-L.L. Wang, Cell locomotion and focal adhesions are regulated by substrate flexibility, Proc. Natl. Acad. Sci. USA 94 (1997) 13661–13665, https://doi.org/10.1073/pnas.94.25.13661.
[59] S. Munevar, Y.L. Wang, M. Dembo, Traction force microscopy of migrating normal and H-ras transformed 3T3 fibroblasts, Biophys. J. 80 (2001) 1744–1757, https://doi.org/10.1016/S0006-3495(01)76145-0.
[60] G.R. Ramirez-San Juan, P.W. Oakes, M.L. Gardel, Contact guidance requires spatial control of leading-edge protrusion, Mol. Biol. Cell 28 (2017) 1043–1053, https://doi.org/10.1091/mbc.E16-11-0769.
[62] S. Torrino, E.M. Grasset, S. Audebert, I. Belhadj, C. Lacoux, M. Haynes, S. Pisano, S. Abélanet, F. Brau, S.Y. Chan, B. Mari, W.M. Oldham, A.J. Ewald, T. Bertero, Mechano-induced cell metabolism promotes microtubule glutamylation to force metastasis, Cell Metabol. 33 (2021) 1342–1357.e10, https://doi.org/10.1016/j.cmet.2021.05.009.
[63] B.P. Liu, M. Chrzanowska-Wodnicka, K. Burridge, Microtubule depolymerization induces stress fibers, focal adhesions, and DNA synthesis via the GTP-binding protein Rho, Cell Adhes. Commun. 5 (1998) 249–255, https://doi.org/10.3109/15419069809040295.
[64] N.B.M. Rafiq, Y. Nishimura, S.V. Plotnikov, V. Thiagarajan, Z. Zhang, S. Shi, M. Natarajan, V. Viasnoff, P. Kanchanawong, G.E. Jones, A.D. Bershadsky, A mechano-signalling network linking microtubules, myosin IIA filaments and integrin-based adhesions, Nat. Mater. 18 (2019) 638–649, https://doi.org/10.1038/s41563-019-0371-y.
[65] A. Kopf, J. Renkawitz, R. Hauschild, I. Girkontaite, K. Tedford, J. Merrin, O. Thorn-Seshold, D. Trauner, H. Häcker, K.D. Fischer, E. Kiermaier, M. Sixt, Microtubules control cellular shape and coherence in amoeboid migrating cells, J. Cell Biol. 219 (2020), e201907154, https://doi.org/10.1083/JCB.201907154.
[66] R.G. Harrison, On the stereotropism of embryonic cells, Science 34 (1911) 279–281, https://doi.org/10.1126/science.34.870.279.
[67] A.S. Zhovmer, E.D. Tabdanov, H. Miao, H. Wen, J. Chen, X. Luo, X. Ma, P.P. Provenzano, R.S. Adelstein, The role of nonmuscle myosin 2A and 2B in the regulation of mesenchymal cell contact guidance, Mol. Biol. Cell 30 (2019) 1961, https://doi.org/10.1091/mbc.E19-01-0071. –1973.
[68] F. Gaertner, P. Reis-Rodrigues, I. de Vries, M. Hons, J. Aguilera, M. Riedl, A. Leithner, S. Tasciyan, A. Kopf, J. Merrin, V. Zheden, W.A. Kaufmann, R. Hauschild, M. Sixt, WASp triggers mechanosensitive actin patches to facilitate immune cell migration in dense tissues, Dev. Cell 57 (2022) 47–62.e9, https://doi.org/10.1016/j.devcel.2021.11.024.
[69] E.D. Tabdanov, A.S. Zhovmer, V. Puram, P.P. Provenzano, Engineering elastic nano- and micro-patterns and textures for directed cell motility, STAR Protoc 1 (2020), 100013, https://doi.org/10.1016/j.xpro.2019.100013.
[70] B.P. Bouchet, R.E. Gough, Y.C. Ammon, D. van de Willige, H. Post, G. Jacquemet, A.F. Maarten Altelaar, A.J.R. Heck, B.T. Goult, A. Akhmanova, Talin-KANK1 interaction controls the recruitment of cortical microtubule stabilizing complexes to focal adhesions, Elife 5 (2016) e18124, https://doi.org/10.7554/eLife.18124.
[71] P. Rougerie, L. Pieuchot, R.S. dos Santos, J. Marteau, M. Bigerelle, P.F. Chauvy, M. Farina, K. Anselme, Topographical curvature is sufficient to control epithelium elongation, Sci. Rep. 10 (2020) 14784, https://doi.org/10.1038/s41598-020-70907-0.
[72] M.E. Pallarès, I. Pi-jaumà, I.C. Fortunato, V. Grazu, M. Gómez-González, P. Roca-cusachs, J.M. De Fuente, R. Alert, R. Sunyer, J. Casademunt, X. Trepat, Stiffness-dependent active wetting enables optimal collective cell durotaxis, Nat. Phys. 19 (2022) 279–289, https://doi.org/10.1038/s41567-022-01835-1.
[73] V. Gkretsi, T. Stylianopoulos, Cell adhesion and matrix stiffness: coordinating cancer cell invasion and metastasis, Front. Oncol. 8 (2018) 145, https://doi.org/10.3389/fonc.2018.00145.